



24



25 **Abstract.** Arctic sea ice decrease in extent in recent decades has been linked to sea surface
26 temperature (SST) anomalies in the North Pacific Ocean. In this study, we assess the relative
27 contributions of the two leading modes in the North Pacific SST anomalies representing external
28 forcing related to global warming and internal forcing related to Pacific Decadal Oscillation (PDO)
29 to the Arctic sea ice loss in boreal summer and autumn. For the 1979-2017 period, the time series
30 of the global warming and PDO modes show significant positive and negative trends, respectively.
31 The global warming mode accounts for 44.9% and 50.1% of the Arctic sea ice loss in boreal
32 summer and autumn during this period, compared to the 20.0% and 22.2% from the PDO mode.
33 There is also a seasonal difference in the response of atmospheric circulations to the two modes.
34 The PDO mode excites a wavetrain from the North Pacific to the Arctic; the wavetrain is not seen
35 in the response of atmospheric circulation to the global warming mode. Both dynamic and
36 thermodynamic forcings work in the relationship of atmospheric circulation and sea ice anomalies.

37

38

39

40

41

42

43

44

45

46



47 1 Introduction

48 Accompanying the abrupt Arctic warming, Arctic sea ice has exhibited a sharp decline trend
49 in recent decades. To explain the Arctic sea ice loss, researchers have proposed a variety of
50 feedback mechanisms, including ice-albedo feedback (Flanner et al., 2011), water vapor and
51 cloud-radiative feedback (Sedlar et al., 2011), and atmospheric lapse-rate feedback (Bintanja et al.
52 2011; Pithan and Mauritsen, 2014). These feedback mechanisms exert effects on Arctic sea ice in
53 the context of the changes in both the anthropogenic forcing and the large-scale circulations. In
54 this study, we assess the impacts of these two factors on Arctic sea ice loss.

55 The anthropogenic factor mainly includes greenhouse gas and aerosol emissions. The
56 increase in greenhouse gas concentrations and the overall decrease in aerosol emissions have been
57 linked to the observed Arctic sea ice loss (Min et al., 2008; Notz and Marotzke, 2012; Gagné et al.
58 2015). The natural factor, mainly changes of large-scale atmospheric and oceanic circulations, has
59 also contributed to the Arctic sea ice decline. The decrease in Arctic sea ice extent has been linked
60 to a positive trend in the North Atlantic Oscillation (NAO) (Deser et al., 2000), the Arctic
61 Oscillation (AO) (Rigor et al., 2002) and the Arctic Dipole (AD) (Wang et al. 2009) indices. The
62 multidecadal variability of sea surface temperature (SST) in the North Pacific and Atlantic Oceans
63 referred to as the Pacific Decadal Oscillation (PDO, Mantua et al., 1997) and the Atlantic
64 Multidecadal oscillation (AMO, Enfield, 2001) also have a strong influence on Arctic sea ice by
65 affecting atmospheric circulation and oceanic heat transfer (Woodgate et al., 2012; Ding et al.,
66 2014; Yu et al., 2017; 2019; Zhang, 2015).

67 It is difficult to separate the contributions of natural (internal) and anthropogenic (external)
68 forcings to the Arctic sea ice decline. General circulation models (GCM) have been applied to



69 assess the relative contributions of these forcings and GCM simulations have suggested a
70 contribution from internal forcing ranging from 20% to 50% over the last three decades (Stroeve
71 et al., 2007; Kay et al., 2011; Day et al., 2012; Ding et al., 2019). However, results from GCMs
72 have been found to underestimate the observed Arctic sea ice loss (Winton, 2011; Stroeve et al.,
73 2012; Mahlstein and Knutti, 2012) due possibly to low sea ice sensitivity to greenhouse gas
74 emissions (Notz and Stroeve, 2016; Rosenblum and Eisenman, 2017) and internal climate
75 variability (Kay et al., 2011; Stroeve et al., 2012; Notz, 2014; Swart et al., 2015).

76 A recent study noted a close connection between the Arctic sea ice loss and the changes in
77 SST in the North Pacific Ocean (Yu and Zhong, 2018) in recent decades. The main modes of
78 variability in the North Pacific SST include the global warming mode, PDO mode (Wills et al.,
79 2018) and Victoria mode (Bond et al., 2003). The relative contributions of these modes to Arctic
80 sea ice loss remain unclear. In this study, we examine the contribution of the global warming and
81 PDO modes, whose time coefficients show significant trends, to the Arctic sea ice loss in boreal
82 summer and autumn during 1979-2017. We will show that the global warming modes in summer
83 and autumn contribute to 44 and 50%, respectively, of Arctic sea ice loss in these seasons; while
84 the respective percentages for the PDO mode are 20 and 22%.

85

86 2 Methodology

87 The National Snow and Ice Data Center (NSIDC) provides Arctic sea ice concentration data
88 (<http://nsidc.org/data/NSIDC-0051>) on a 25 km × 25 km grid with a polar stereographic projection
89 from October 1979 to the present. Although the sea ice data have some defects from surface
90 flooding (Comiso and Steffen, 2001) and land contamination and weather (Cavalieri et al., 1999),



91 they can be applicable to the study of changes of Arctic sea ice concentration. The current analyses
 92 use monthly data from boreal summer (June-August) and autumn (September - November).
 93 Atmospheric variables are derived from the European Centre for Medium-Range Weather
 94 Forecasts (ECMWF) ERA-Interim reanalysis (Dee et al., 2011), which has a horizontal resolution
 95 of 79 km (T255) at 60 vertical levels. ERA-Interim reanalysis outperforms other contemporary
 96 global reanalysis datasets, even though it has a warm and moist bias in the planetary boundary
 97 layer (Jakobson et al., 2012). The North Pacific SST patterns are derived from the 2° latitude \times 2°
 98 longitude U.S. National Oceanic and Atmospheric Administration (NOAA) Extended
 99 Reconstructed SST data (<http://ftp.cdc.noaa.gov/noaa.ersst.v5>), which is superior in high latitudes
 100 to other SST datasets (Huang et al., 2017).

101 The empirical orthogonal function (EOF) method is employed to obtain the global warming
 102 and PDO modes considered as the first two modes. The EOF modes include spatial patterns (EOFs)
 103 and corresponding time coefficients or principal components (PCs) characterized with
 104 orthogonality with each other. The global warming signal and the PDO index correspond to the
 105 time series of the first two modes of the SST anomalies in the North Pacific north of 20° N. The
 106 statistical significance level is tested by the Student's t- test.

107

108 **3 Results**

109 **3.1 Arctic sea loss explained by the first two EOF modes**

110 We first present the trends in the North Pacific SST in boreal summer and autumn (Figure 1a
 111 and 1b). Warming trends dominate over the whole study region with significant ones in the
 112 western and central North Pacific. As an important climate mode of the North Pacific, PDO may



113 contribute to the warming trend. The PDO indices (<http://research.jisao.washington.edu/pdo>) show
 114 statistically significant negative trends of -0.0293 ($p < 0.05$) and -0.0261 yr^{-1} ($p < 0.1$) respectively
 115 for boreal summer and autumn (Figure 1c and 1d).

116 The results of EOF analysis of the North Pacific SST anomalies in boreal summer and autumn
 117 are shown in Figure 2 and 3. The first mode (EOF1) of the summer SST and the second mode
 118 (EOF2) of the autumn SST, explaining 29.6% and 19.6% of total variance, show a nearly uniform
 119 warming pattern in the North Pacific. An increasing trend in the time series for these two EOF
 120 modes (PC1 for summer and PC2 for autumn) represents a global warming mode (Wills et al.,
 121 2018). The warming trends at 0.0623 and 0.0645 per year ($p < 0.05$) for summer and autumn,
 122 respectively, are not steady with a warming hiatus between 1998 and 2012, flanked by two rapid
 123 warming periods. The domain-averaged warming trends in the North Pacific SST are the same for
 124 summer and autumn, at $0.94 \text{ }^{\circ}\text{C}$ per century. Trenberth and Shea (2006) considered the global
 125 mean SST as a proxy for external signal. The global mean SST is significantly correlated with
 126 summer PC1 (correlation coefficient 0.79 , $p < 0.05$) and autumn PC2 (0.84 , $p < 0.05$), suggesting
 127 that these global warming modes in SST is likely to represent an external signal.

128 The second mode of summer SST and the first mode of autumn SST, accounting for 21.4%
 129 and 27.8% of the total variance for the respective season, represent the positive phase of the PDO
 130 mode, which has negative SST anomalies over the mid-latitudes surrounded by positive SST
 131 anomalies. The time series of these two SST modes, referred as the PDO mode, are highly
 132 correlated with the PDO index with the correlation coefficients of 0.97 between the summer PC2
 133 and PDO and 0.94 between the autumn PC1 and PDO. The PCs of the PDO mode alter from
 134 positive phase with the mean index value of 0.49 before 1998, to negative phase with the mean



135 value of -0.51 afterwards. The trends in the PCs of the PDO mode are -0.0334 and -0.0349 per
 136 year for summer and autumn ($p < 0.05$).

137 Next, we assess the response of Arctic sea ice to the global warming (external) and PDO
 138 (internal) modes, by regressing the Arctic sea ice anomalies onto summer PC1 and autumn PC2
 139 (global warming mode) and to summer PC2 and autumn PC1 (PDO mode) (Figure 4). In both
 140 seasons, the global warming mode is associated with Arctic sea ice loss (Figure 4a and 4d). The
 141 regions with strongest association span the eastern side from Barents Sea to East Siberian,
 142 Chukchi and Beaufort Seas. While the season changes from summer to autumn when Arctic sea
 143 ice is at the minimum value, the region of the largest decrease related to the global warming mode
 144 shifts from the northern Barents Sea to East Siberian and Chukchi Seas. In contrast, the PDO
 145 modes correspond to positive Arctic sea ice anomalies (Figure 4b and 4c). Compared to the global
 146 warming mode, the associations between the PDO mode representing the positive PDO phase and
 147 the Arctic sea ice anomalies are somewhat weaker from Greenland Sea to Beaufort Sea, but
 148 stronger in Baffin Bay, Hudson Bay and the sea near Queen Elizabeth Islands. For both the global
 149 warming mode and the PDO mode, the connection is somewhat stronger in autumn than summer.

150 Sea ice concentration show a decreasing trend everywhere north of 50°N except for some
 151 coastal regions of Greenland (Figure 5). Similar to the negative sea ice anomalies related to the
 152 global warming mode in SST that are larger in values in autumn than summer, negative sea ice
 153 trends are also somewhat sharper in autumn than those in summer and the largest negative trends
 154 move from Barents Sea in summer to East Siberian and Chukchi Seas in autumn. The
 155 contributions of the global warming mode and the PDO mode to the total trends in summer and
 156 autumn Arctic sea ice, which is calculated by the product of regression coefficients of sea ice into



the PC (Figure 4) and the trends in the PC (Figures 2 and 3) are shown in Figure 6. Both modes contribute to Arctic sea ice trends in the two seasons, but the amount of the contribution differs, with the largest contribution from the autumn global warming mode and the smallest one from the summer PDO mode. The relative contribution can be also assessed by a contribution ratio calculated as the ratio of trends explained by the two modes (Figure 6) to the total trends (Figure 5) and the results at grid points where the trends are significant and the contribution ratio is greater than 0.001 yr^{-1} are shown in Figure 7. The contribution ratios from the global warming mode are larger than those from the PDO mode with the exception of Hudson Bay in summer. The domain-averaged contribution ratios from the global warming mode and the PDO mode are 44.9% and 20.0%, respectively, in summer and 50.0% and 22.2% in autumn.

167

3.2 Mechanisms

The relationship between the Arctic sea ice trends and the first two modes of the North Pacific SST variability merits further consideration in the context of large-scale circulations. Regression analyses are performed where the 500-hPa geopotential height, mean sea level pressure (MSLP), 850-hPa wind, and surface temperature are regressed into the PCs of the two modes in summer and autumn and the results are shown in Figures 8-11. In summer, the regression patterns of the anomalous 500-hPa height and MSLP onto the global warming mode resemble the positive phase of the NAO and AO (Figure 8a and 9a), which show a nearly barotropic structure. The positive 500-hPa height and MSLP anomalies over the Bering Sea produce an anticyclonic circulation (Figure 10a), which transports warm air into the Pacific sector of the Arctic, leading to positive temperature anomalies (Figure 11a) and negative sea ice anomalies there (Figure 4a). The



179 southerly winds also move the sea ice towards the North Pole, thus resulting in sea ice loss in the
180 Chukchi Sea. The northerly winds over the northeastern Canada and northern Greenland (Figure
181 10a) advect warm air to the Kara and Barents Seas, increasing surface air temperature (Figure 11a)
182 and decreasing sea ice concentration there.

183 In contrast to summer, the regression pattern in autumn is dominated by positive
184 500-hPa height anomalies across the Arctic with the exception of northeastern Canada and western
185 Greenland (Figure 8d). However the anomalous MSLP regression map displays a noticeable
186 positive phase of the AO index (Figure 9d). The baroclinic structure in autumn differs from the
187 barotropic feature in summer. The positive MSLP anomalies over the Bering Sea and negative
188 MSLP anomalies over the Chukchi and East Siberian Seas are favorable for warm air flowing into
189 the Arctic (Figure 10d), which is related to increasing air temperature (Figure 11d) and decreasing
190 sea ice over the Pacific sector of the Arctic (Figure 4d). The negative MSLP anomalies over
191 Greenland and positive MSLP anomalies over Northern Europe induce southwesterly winds over
192 North Atlantic Ocean extending to most of the Arctic resulting in more significant warming and
193 Arctic sea ice loss in autumn than in summer. Although the anomalous North Pacific SST patterns
194 related to the global warming mode are similar in summer and autumn, the corresponding
195 atmospheric circulations patterns are different, and produce noticeable differences in the pattern of
196 surface air temperature increases and sea ice loss in the Arctic.

197 In boreal summer, the positive phase of the PDO mode is related to a Rossby wavetrain
198 extending from the North Pacific and North America to the Arctic Ocean and Europe (Figure 8b).
199 Throughout the Arctic, negative anomalies in 500-hPa height and MSLP dominate, corresponding
200 to slightly positive phase of the AO index (Figure 9b). The anomalous southerly winds induced by



201 the negative MSLP over Greenland produce negligible warming in the northern North Atlantic and
202 central Arctic (Figure 10b). On the contrary, northerly winds from the North Pole generate
203 significant cooling in terrestrial Arctic and northeastern Canadian archipelago (Figure 11b), where
204 sea ice concentration increases significantly (Figure 4b). Meanwhile the northerly winds drive the
205 sea ice into the surrounding seas, leading to the increase in sea ice concentration there.

206 In autumn, the wavetrain occurs over the North Pacific, North America, and North Atlantic
207 (Figure 8c). The positive MSLP anomalies produce increasing (decreasing) air temperature and
208 decreasing (increasing) sea ice over Greenland and the Greenland Sea (Barents Sea), related to
209 anomalous southerly (northerly) winds (Figure 9c, 10c, 11c and 4c). Over the Laptev and East
210 Siberian Seas, anomalous northerly winds also generate significant cooling and sea ice increase.
211 The anomalous high moves from Bering Strait to the Gulf of Alaska, which limits the warming
212 into the Arctic Ocean. Thus the Pacific sector of the Arctic shows a cooling tendency and
213 increasing sea ice concentration. Similar to the global warming mode, the PDO mode also shows a
214 seasonal feature in its effect on atmospheric circulation and sea ice with more significant influence
215 in autumn than summer. The response of atmospheric circulation to the PDO mode shows a more
216 barotropic structure than the response to the global warming mode.

217

218 **4 Discussion and Conclusions**

219 Following the suggestion that the North Pacific SST anomalies play an important role in the
220 melt season Arctic sea ice loss (Yu and Zhong, 2018), the current study further assesses the
221 relative contribution of the two leading EOF modes in SST variability, representing the global
222 warming (external) and PDO (internal) modes, to the trends in Arctic sea ice in boreal summer and



223 autumn for the recent four decades (1979-2017). As the first two modes of the North Pacific SST
224 variability, the time coefficients of the global warming (summer PC1 and autumn PC2) and the
225 PDO (summer PC2 and autumn PC1) modes exhibit a significant increasing and decreasing trend,
226 respectively. In summer, the PDO and global warming modes contribute to 20.0% and 44.9% of
227 Arctic sea ice loss, respectively; while in autumn the percentages are 22.2% and 50.1%. Both
228 modes also exert more significant effects on large-scale atmospheric circulations in autumn than in
229 summer. The response of corresponding atmospheric circulations to the two modes also differs in
230 summer and autumn, especially over northern North Atlantic. In contrast to summer, the autumn
231 anomalous atmospheric circulations related to the global warming mode are more baroclinic. For
232 the PDO mode, the wavetrain propagates more eastwards in summer than in autumn. The
233 anomalous surface wind fields related to the two modes perturb the dynamic and thermodynamic
234 environments in ways that are consistent with the observed patterns of the Arctic sea ice change.

235 Previous studies investigating the contributions of external and internal forcings to Arctic sea
236 ice loss have been based heavily on numerical modeling. Model results, however, have shown
237 large departures from observations in the Arctic due to the lack of understanding in sea ice
238 dynamics and thermodynamics and their interactions with the atmosphere and other uncertainties
239 in physical parameterizations and numerical algorithms (Winton, 2011; Stroeve et al., 2012;
240 Mahlstein and Knutti, 2012). The results here are based on reanalysis products which are
241 considered more reliable than model outputs because of the assimilation of in-situ observations
242 and remote sensing satellite data. Previous studies have suggested that internal forcing may
243 explain somewhere between 20% to 50% of Arctic sea ice loss (Stroeve et al., 2007; Kay et al.,
244 2011; Day et al., 2012; Ding et al., 2019). Our results show that internal forcing represented by the



245 PDO mode contributes to slightly more than 20% of the Arctic sea ice loss in summer and autumn
246 and thus total contribution from internal factors must exceed 20%.

247 In addition to PDO, the AMO mode is also found to be important to the Arctic sea ice loss
248 through its effect on oceanic and atmospheric heat transport (Yu et al., 2017; Zhang, 2015). Day et
249 al. (2012) attributed 5-30% of Arctic sea loss to the AMO mode. It must be cautioned that the parts
250 of the global warming mode should be removed when estimating the contribution of the AMO
251 mode to the Arctic sea ice loss (Ting et al., 2009). Besides SST in the North Pacific and Atlantic,
252 other important factors for Arctic sea ice loss in summer and autumn include the effects of
253 atmospheric internal variability on heat and moisture transports from mid-latitudes to the Arctic
254 (Kapsch et al., 2013; Naakka et al., 2019).

255 In this study, the contribution of the global warming mode to the Arctic sea ice depletion is
256 explained in the context of atmospheric circulation anomalies. The effect of the global warming
257 mode also work directly through some local feedback processes (Vihma et al., 2014), including
258 ice-albedo feedback (Flanner et al., 2011), water vapor and cloud-radiative feedback (Sedlar et al.,
259 2011), and processes related to lower atmosphere stability such as surface inversion (Bintanja et al.
260 2011; Pithan and Mauritsen, 2014). The external forcing also may interact with the
261 above-mentioned internal forcing (Ding et al., 2019). The global warming mode considered here
262 combines all anthropogenic factors, including greenhouse gas, aerosols, and ozone. The data and
263 analysis tools used in this study are unable to separate their individual contributions.

264

265

266



267 *Author contributions.* LY designed the study and analyzed the data. All authors discussed the
268 results and contributed to the writing and editing of the manuscript.

269 *Competing interests.* All authors declare that they have no conflict of interest.

270 *Acknowledgements.* We thank the agencies for providing the datasets used in this study. This work
271 was supported by the National Key R&D Program of China (No. 2017YFE0111700) and the
272 Academy of Finland (contract 317999).

273

274

275

276

277

278

279

280

281

282

283

284

285

286

287

288



289 References

- 290 Bintanja, R., Graverson, R. G., and Hazeleger, W.: Arctic winter warming amplified by the
291 thermal inversion and consequent low infrared cooling to space, *Nat Geosci.*, 4, 758-761,
292 doi:10.1038/ngeo1285, 2011.
- 293 Bond, N. A., Overland, J. E., Spillane, M., and Stabeno, P. J.: Recent shifts in the state of the
294 North Pacific. *Geophys. Res. Lett.*, 30, 2183, 2003.
- 295 Cavalieri, D. J., Parkinson, C. L., Gloersen, P., Comiso, J. C., and Zwally, H. J.: Deriving
296 long-term time series of sea ice cover from satellite passive-microwave multisensory data
297 sets, *J. Geophys. Res.*, 104, 15803–15814, doi: 10.1029/1999jc900081, 1999.
- 298 Comiso, J. C., and Steffen, K.: Studies of Antarctic sea ice concentrations from satellite data and
299 their applications, *J. Geophys. Res.*, 106, 31361–31385, doi:10.1029/2001JC000823, 2001.
- 300 Day, J. J., Hargreaves, J. C., Annan, J. D. and Abe-Ouchi, A.: Sources of multi-decadal variability
301 in Arctic sea ice extent, *Environ. Res. Lett.*, 7, 03011, doi:10.1088/1748-9326/7/3/034011,
302 2012.
- 303 Dee, D. Uppala, S., Simmons, A., Berrisford, P., Poli, P., Kobayashi, S., Andrae, U., Balmaseda,
304 M., Balsamo, G., Bauer, P., Bechtold, P., Beljaars, A., van de Berg, L., Bidlot, J., Bormann,
305 N., Delsol, C., Dragani, R., Fuentes, M., Geer, A., Haimberger, L., Healy, S., Hersbach, H.,
306 Hódin, E., Isaksen, I., Kållberg, P., Köhler, M., Matricardi, M., McNally, A., Monge-Sanz, B.,
307 Morcrette, J., Park, B., Peubey, C., de Rosnay, P., Tavolato, C., Thépaut, J., and Vitart, F.: The
308 ERA-Interim reanalysis: configuration and performance of the data assimilation system, *Q. J.*
309 *Roy. Meteor. Soc.*, 137, 553-597, doi:10.1002/qj.828, 2011.
- 310 Deser, C., Walsh, J. E., and Timlin, M. S.: Arctic sea ice variability in the context of recent



- 311 atmospheric circulation trends, *J. Climate*, 13, 617-633,
- 312 doi:10.1175/1520-0442(2000)013<0617:ASIVIT>2.0.CO;2, 2000.
- 313 Ding, Q., Wallace, J. M., Battisti, D. S., Steig, E. J., Gallant, A. J. E., Kim, H.-J., and Geng, L.:
314 Tropical forcing of the recent rapid Arctic warming in northeastern Canada and Greenland,
315 *Nature*, 509, 209-212, doi:10.1038/nature13260, 2014.
- 316 Ding, Q., Schweiger, A., L'Heureux, M., Steig, E. J., Battisti, D. S., Johnson, N. C.,
317 Blanchard-Wrigglesworth, E., Po-Chedley, S., Zhang, Q., Harnos, K., Bushuk, M., Markle,
318 B., and Baxter, I.: Fingerprints of internal drivers of Arctic sea ice loss observations and
319 model simulations, *Nature Geoscience*, 12, 28-33, doi:10.1038/s41561-018-0256-8, 2019.
- 320 Enfield, D. B., Mestas-Nunez, A. M., and Trimble, P. J.: The Atlantic Multidecadal Oscillation
321 and its relationship to rainfall and river flows in the continental U.S., *Geophys. Res. Lett.*,
322 28, 2077-2080, doi:10.1029/2000gl012745, 2001.
- 323 Flanner, M. G., Shell, K. M., Barlage, M., Perovich, D. K., and Tschudi, M. A.: Radiative forcing
324 and albedo feedback from the Northern Hemisphere cryosphere between 1979 and 2008,
325 *Nat. Geosci.*, 4, 151–155, doi:10.1038/ngeo1062, 2011.
- 326 Gagné M.-È., Gillett, P. N., and Fyfe, J. C.: Impact of aerosol emission controls on future arctic
327 sea ice cover, *Geophys. Res. Lett.*, 42, 8481-8488, doi:10.1002/2015GL065504, 2015.
- 328 Huang, B., Thorne, P. W., Banzon, V. F., Boyer, T., Chepurin, G. A., Lawrimore, J. H., Menne, M.
329 J., Smith, T. M., Vose, R. S., and Zhang, H.-M.: Extended Reconstructed Sea Surface
330 Temperature version 5 (ERSSTv5), Upgrades, validations, and intercomparisons, *J. Climate*,
331 30, 8179-8205, doi:10.1175/JCLI-D-16-0836.1, 2017.
- 332 Jakobson, E., Vihma, T., Palo, T., Jakobson, L., Keernik, H., and Jaagus, J.: Validation of



- 333 atmospheric reanalyses over the central Arctic Ocean, *Geophys. Res. Lett.*, 39,
334 L10802, doi:10.1029/2012GL051591, 2012.
- 335 Kapsch, M.-L., Graverson, R. G., and Tjernström, M.: Springtime atmospheric energy transport
336 and the control of Arctic summer sea-ice extent, *Nature Climate Change*, 3, 744–748,
337 doi:10.1038/nclimate1884, 2013.
- 338 Kay, J. E., Holland, M. M., and Jahn, A.: Inter-annual to multi-decadal Arctic sea ice extent trends
339 in a warming world, *Geophys. Res. Lett.*, 38, L15708, doi:10.1029/2011GL048008, 2011.
- 340 Mahlstein, I., and Knutti, R., September Arctic seaice predicted to disappear near 2 °C global
341 warming above present, *J. Geophys. Res.*, 117, D06104, doi:10.1029/2011JD016709, 2012.
- 342 Min, S.-K., Zhang, X., Zwiers, F. W., and Agnew, T.: Human influence on arctic sea ice detectable
343 from early 1990s onwards, *Geophys. Res. Lett.*, 35, 213–36, doi: 10.1029/2008gl035725,
344 doi:10.1029/2008GL035725, 2008.
- 345 Mantua, N. J., Hare, S. R., Zhang, Y., Wallace, J. M., and Francis, R. C.: A Pacific interdecadal
346 climate oscillation with impacts on salmon production, *Bull. Amer. Meteor. Soc.*, 78,
347 1069–1079, doi:10.1175/1520-0477(1997)078<1069:APICOW>2.0.CO;2, 1997.
- 348 Naakka, T., Nygård, T., Vihma, T., Graverson, R., and Sedlar, J.: Atmospheric moisture transport
349 between mid-latitudes and the Arctic: regional, seasonal and vertical distributions, *Int. J.*
350 *Climatol.*, doi:10.1002/joc.5988, 2019.
- 351 Notz, D., and Marotzke, J.: Observations reveal external driver for Arctic sea-ice retreat.
352 *Geophys. Res. Lett.*, 39, 89–106, doi: 10.1029/2012GL051094, 2012.
- 353 Notz, D.: Sea-ice extent and its trend provide limited metrics of model performance, *The*
354 *Cryosphere*, 8, 229–243, doi: 10.5194/tc-8-229-2014, 2014.
- 355 Notz, D., and Stroeve, J.: Observed Arctic sea-ice loss directly follows anthropogenic CO₂



- 356 emission, *Science*, 354, 747-750, doi: 10.1126/science.aag2345, 2016.
- 357 Pithan, F., and Mauritsen, T.: Arctic amplification dominated by temperature feedbacks in
- 358 contemporary climate models, *Nat. Geosci.*, 7, 181-184, doi:10.1038/ngeo2071, 2014.
- 359 Rigor, I., Wallace, J. M., and Colony, R. L.: Response of sea ice to the Arctic Oscillation, *J.*
- 360 *Climate*, 15, 2648–2663, doi:10.1175/1520-0442(2002)015<2648:ROSITT>2.0.CO;2, 2002.
- 361 Rosenblum, E. and Eisenman, I.: Sea ice trends in climate models inly accurate in runs with
- 362 biased global warming, *J. Climate*, 30, 6265-6278, doi:10.1175/jcli-d-16-0455.1, 2017.
- 363 Sedlar, J., Tjernström, M., Mauritsen, T., Shupe, M. D., Brooks, I. M., Persson, P. O. G., Birch, C.
- 364 E., Leck, C., Sirevaag, A., and Nicolaus, M.: A transitioning Arctic surface energy budget:
- 365 the impacts of solar zenith angle, surface albedo and cloud radiative forcing, *Clim.*
- 366 *Dyn.*, 37, 1643–1660, doi:10.1007/s00382-010-0937-5, 2011.
- 367 Stroeve, J., Holland, M. M., Meier, W., Scambos, T., and Serreze, M.: Arctic sea ice decline:
- 368 faster than forecast, *Geophys. Res. Lett.*, 34, L09501, doi: 10.1029/2007gl029703, 2007
- 369 Stroeve, J. C., Kattsov, V., Barrett A., Serreze, M., Pavlova, T., Holland, M., and Meier W. N.:
- 370 Trends in Arctic sea ice extent from CMIP5, CMIP3 and observations, *Geophys. Res.*
- 371 *Lett.*, 39, L16502, 10.1029/2012GL052676, 2012,
- 372 Swart, N. C., Fyfe, J. C., Hawkins, E., Kay, J. E., and Jahn, A.: Influence of internal variability on
- 373 Arctic sea-ice trends, *Nat. Climate Change*, 5, 86–89, doi:10.1038/nclimate2483, 2015.
- 374 Ting, M., Kushnir, Y., Seager, R., and Li, C.: Forced and internal twentieth-century SST
- 375 trends in the North Atlantic, *J. Climate*, 22, 1469-1481, doi:10.1175/2008JCLI2561.1, 2009.
- 376 Trenberth, K. E., and Shea, D. J.: Atlantic hurricanes and natural variability in 2005, *Geophys. Res.*
- 377 *Lett.*, 33, L12704, doi:10.1029/2006GL026894, 2006.



- 378 Vihma, T., Pirazzini, R., Fer, I., Renfrew, I. A., Sedlar, J., Tjernström, M., Lüpkes, C., Nygård, T.,
379 Notz, D., Weiss, J., Marsan, D., Cheng, B., Birnbaum, G., Gerland, S., Chechin, D., and
380 Gascard, J. C.: Advances in understanding and parameterization of small-scale physical
381 processes in the marine Arctic climate system: a review. *Atmos. Chem. Phys.*, 14,
382 9403-9450, doi:10.5194/acp-14-9403-2014, 2014.
- 383 Wang, J., Zhang, J., Watanabe, E., Ikeda, M., Mizobata, K., Walsh, J. E., Bai, X., and Wu, B.: Is
384 the Dipole anomaly a major driver to record lows in Arctic summer sea ice extent?,
385 *Geophys. Res. Lett.*, 36, L05706, doi:10.1029/2008GL036706, 2009.
- 386 Wills, R. C., Schneider, T., Wallace, J. M., Battisti, D. S., and Hartmann, D. L.: Disentangling
387 global warming , multidecadal variability, and El Nino in Pacific temperatures, *Geophys.*
388 *Res. Lett.*, 45, 2487-2496, doi:10.1002/2017GL076327, 2018.
- 389 Woodgate, R. A., Weingartner, T. J., and Lindsay, R.: Observed increases in Bering Strait
390 oceanic fluxes from the Pacific to the Arctic from 2001 to 2011 and their impacts on the
391 Arctic Ocean water column, *Geophys. Res. Lett.*, 39, L24603, doi:10.1029/2012GL054092,
392 2012.
- 393 Winton, M.: Do climate models underestimate the sensitivity of Northern Hemisphere sea ice
394 cover?, *J. Climate*, 24, 3924-3934, doi:10.1175/2011JCLI4146.1, 2011.
- 395 Yu, L., Zhong, S., Winkler, J. A., Zhou, M., Lenschow, D. H., Li, B., Wang, X., and Yang, Q.:
396 Possible connection of the opposite trends in Arctic and Antarctic sea ice cover, *Sci. Rep.*, 7,
397 45804, doi:10.1038/srep45804, 2017.
- 398 Yu, L., and Zhong, S.: Changes in sea-surface temperature and atmospheric circulation patterns
399 associated with reductions in Arctic sea ice cover in recent decades, *Atmos. Chem.*



400 Phys., 18, 14149-14159, 2018.

401 Yu L., Zhong, S., Zhou, M., Lenschow, D. H., and Sun, B.: Revisiting the linkages between the

402 variability of atmospheric circulations and Arctic melt-season sea ice cover at multiple time

403 scales, J. Climate, 32, 1461-1482, doi:10.1175/JCLI-D-18-0301.1, 2019.

404 Zhang, R.: Mechanisms for low-frequency variability of summer Arctic sea ice extent. Proc.

405 Natl. Acad. Sci. USA, 112, 4570-4575, doi:10.1073/pnas.1422296112, 2015.

406

407

408

409

410

411

412

413

414

415

416

417

418

419

420

421



422 Figure captions

423 Figure 1. The trends in the North Pacific SST in summer (a) and autumn (b) ($^{\circ}\text{C yr}^{-1}$) and time
 424 series of the PDO indices in summer (c) and autumn (d) for the period 1979-2017. Dotted regions
 425 in Figure (a) and (b) indicate above 95% confidence level. Dashed lines in Figure (c) and (d)
 426 denote the trends in the PDO indices.

427 Figure 2. Spatial patterns (EOF1 and EOF2) and time series (PC1 and PC2) of the leading two
 428 EOF modes of summer North Pacific SST over the region (120°E - 100°W , 20°N - 65°N) during
 429 1979-2017. The number in the left panels indicates the percentage of variance explained by the
 430 two modes. The black dashed lines in the right panels denote the trends for the period 1979-2017.

431 Figure 3. The same as Figure 2, but for autumn.

432 Figure 4. Regression maps of summer (a), (b) and autumn (c), (d) sea ice concentration anomalies
 433 into the time series of the first (a), (c) and second (b), (d) mode of summer (a), (b) and autumn (c),
 434 (d) SST anomalies in the North Pacific. Dotted regions denote above 95% confidence level.

435 Figure 5. Trends in sea ice concentration (yr^{-1}) for summer (a) and autumn (b). Dotted regions
 436 denote above 95% confidence level.

437 Figure 6. Trends in sea ice concentration (yr^{-1}) explained by the first (a), (c) and second (b), (d)
 438 modes of summer (a), (b) and autumn (c), (d) North Pacific SST anomalies.

439 Figure 7. The ratio of trends explained by the first (a), (c) and second (b), (d) modes of summer (a),
 440 (b) and autumn (c), (d) North Pacific SST anomalies. Only grid points where the trends are
 441 significant and more than 0.001 yr^{-1} are shown.

442 Figure 8. Regression maps of 500-hPa geopotential height (gpm) onto the time series of the first
 443 (a), (c) and second (b), (d) mode of summer (a), (b) and autumn (c), (d) North Pacific SST



444 anomalies. Dotted regions indicate above 95% confidence level.

445 Figure 9. The same as Figure 8, but for mean sea level pressure (MSLP) (Pascal).

446 Figure 10. The same as Figure 8, but for 850-hPa wind field.

447 Figure 11. The same as Figure 8, but for surface air temperature (°C).

448

449

450

451

452

453

454

455

456

457

458

459

460

461

462

463

464

465

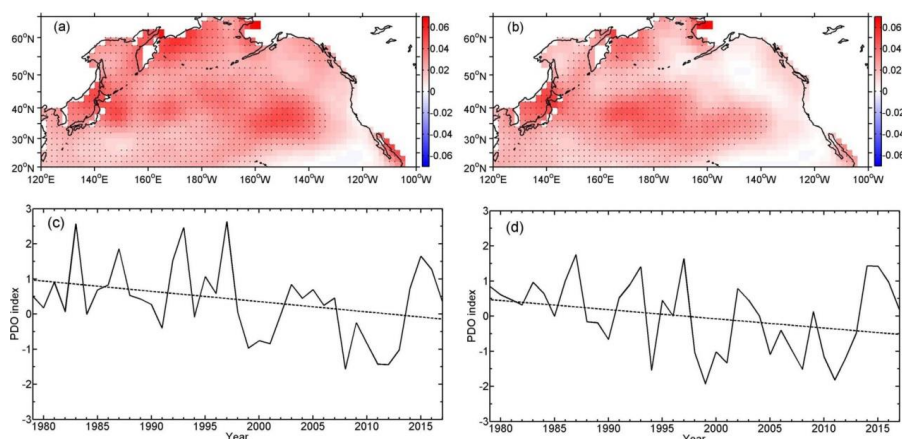


Figure 1. The trends in the North Pacific SST in summer (a) and autumn (b) (°C yr⁻¹) and time series of the PDO indices in summer (c) and autumn (d) for the period 1979-2017. Dotted regions in Figure (a) and (b) indicate above 95% confidence level. Dashed lines in Figure (c) and (d) denote the trends in the PDO indices.

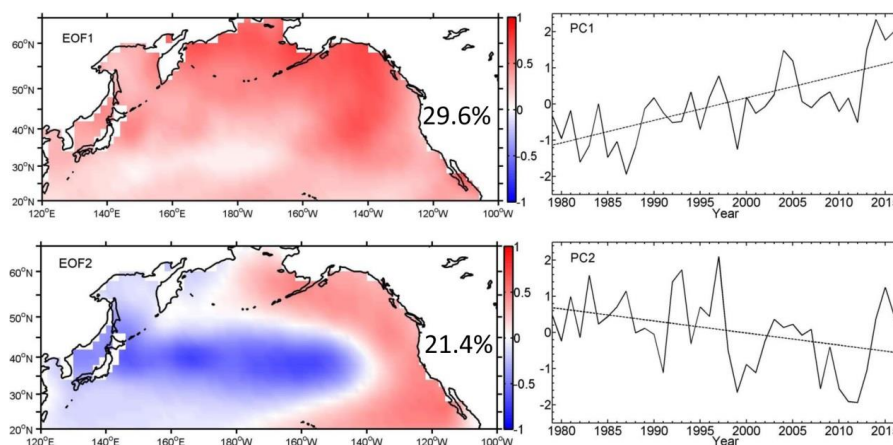


Figure 2. Spatial patterns (EOF1 and EOF2) and time series (PC1 and PC2) of the leading two EOF modes of summer North Pacific SST over the region (120°E–100°W, 20°N–65°N) during 1979–2017. The number in the left panels indicates the percentage of variance explained by the two modes. The black dashed lines in the right panels denote the trends for the period 1979–2017.

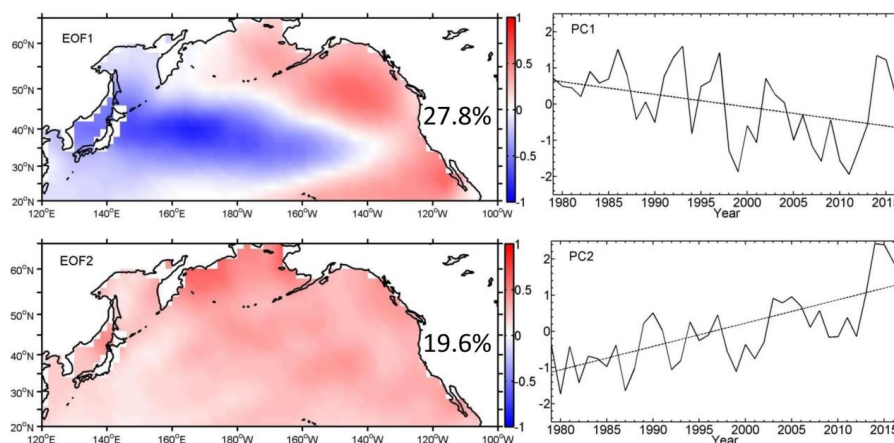


Figure 3. The same as Figure 2, but for autumn.

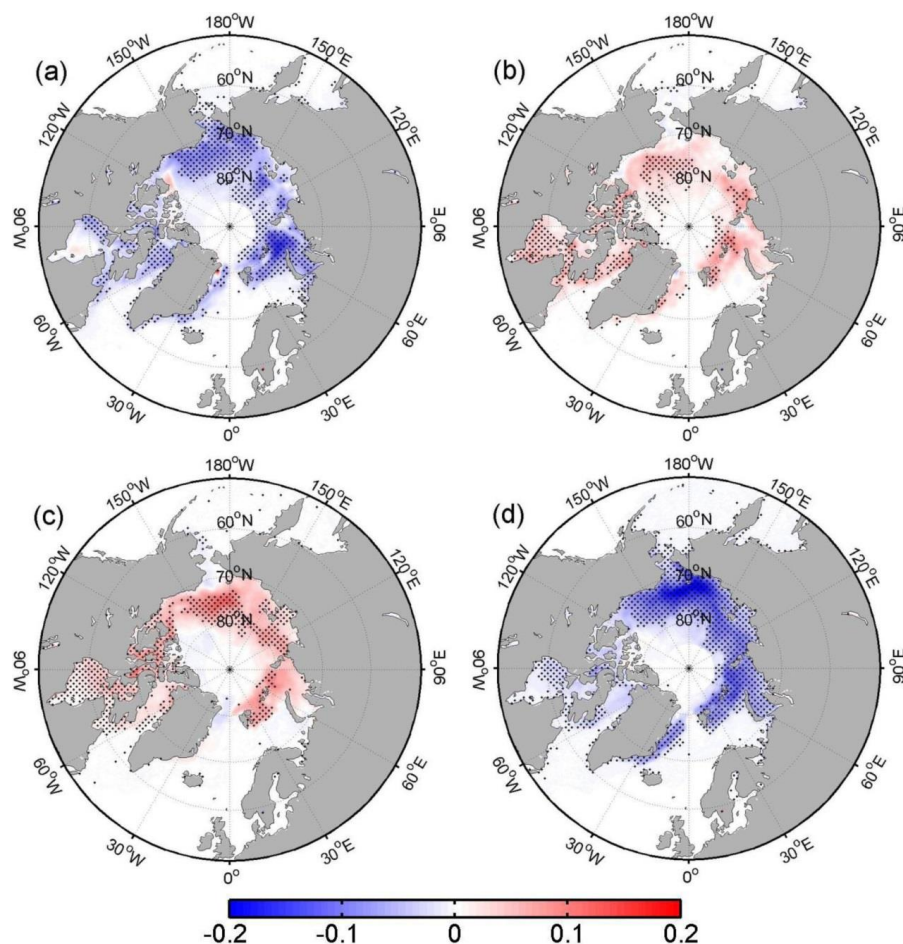


Figure 4. Regression maps of summer (a), (b) and autumn (c), (d) sea ice concentration anomalies into the time series of the first (a), (c) and second (b), (d) mode of summer (a), (b) and autumn (c), (d) SST anomalies in the North Pacific. Dotted regions denote above 95% confidence level.

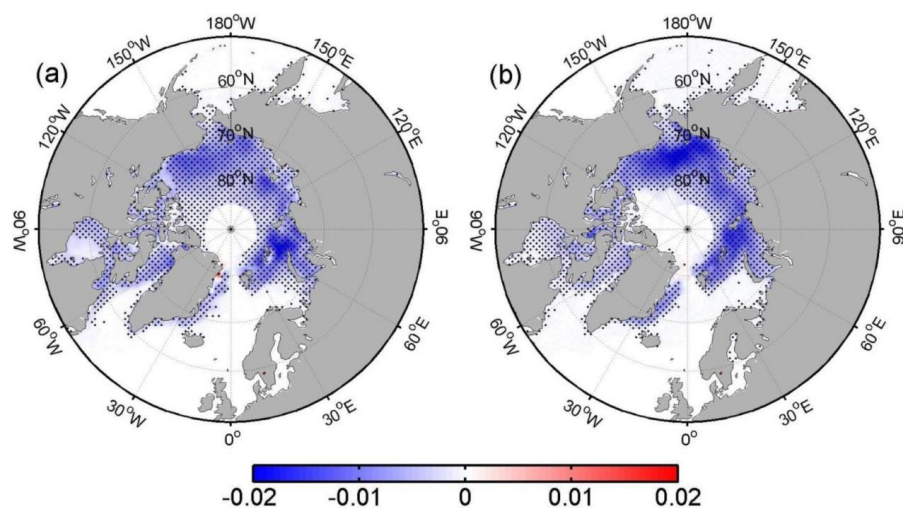


Figure 5. Trends in sea ice concentration (yr^{-1}) for summer (a) and autumn (b). Dotted regions denote above 95% confidence level.

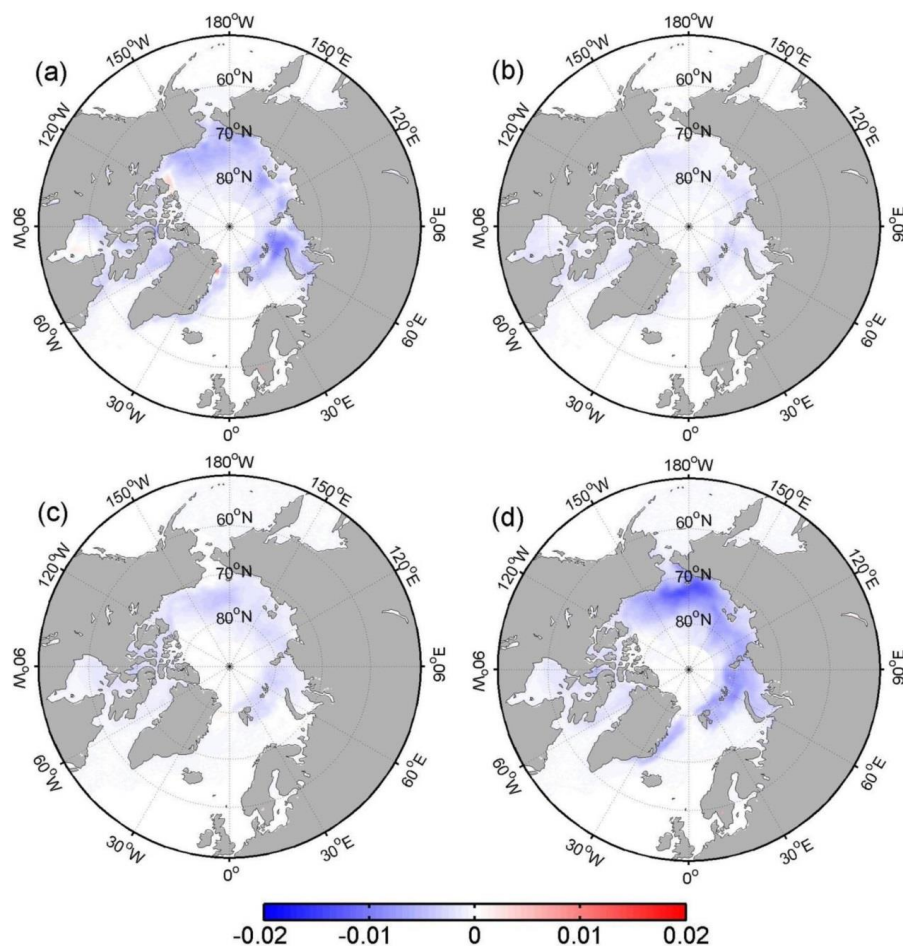


Figure 6. Trends in sea ice concentration (yr^{-1}) explained by the first (a), (c) and second (b), (d) modes of summer (a), (b) and autumn (c), (d) North Pacific SST anomalies.

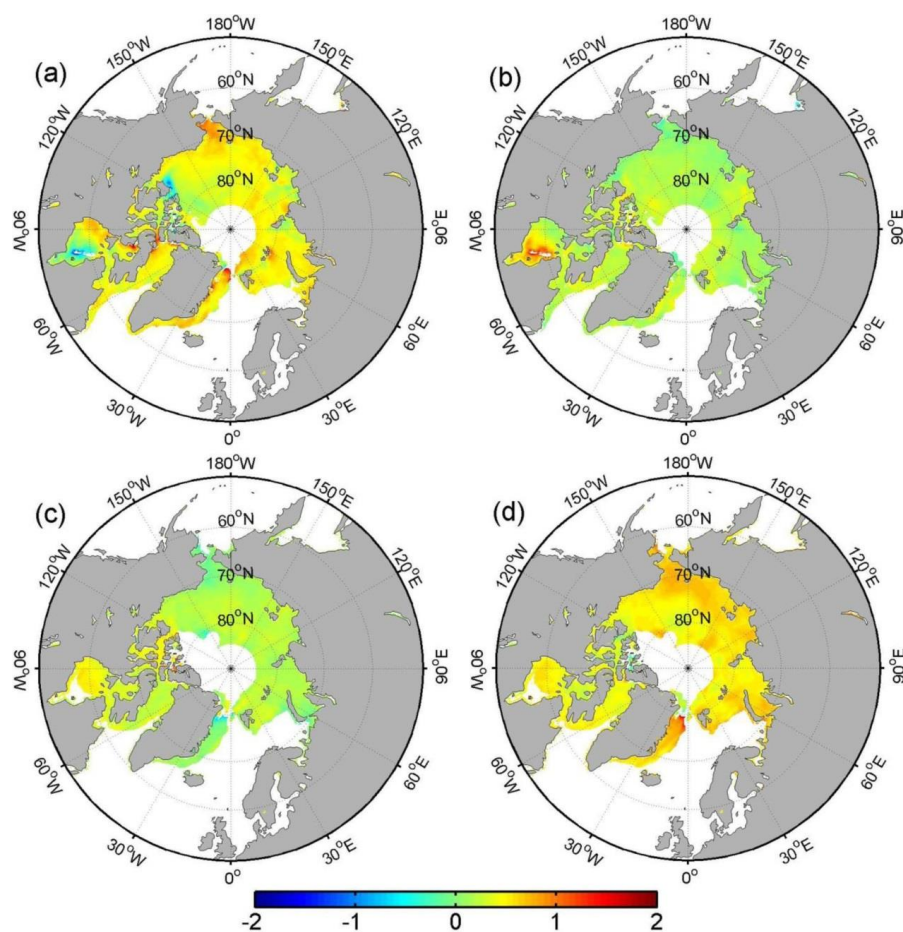


Figure 7. The ratio of trends explained by the first (a), (c) and second (b), (d) modes of summer (a), (b) and autumn (c), (d) North Pacific SST anomalies. Only grid points where the trends are significant and more than 0.001 yr^{-1} are shown.

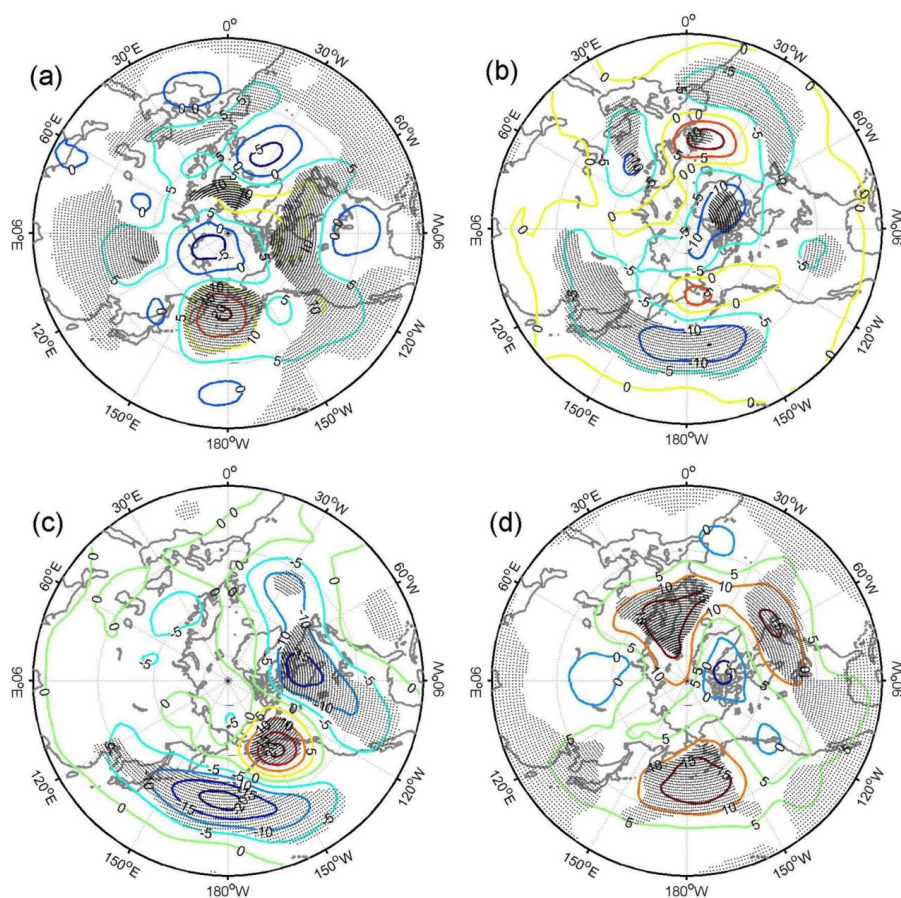
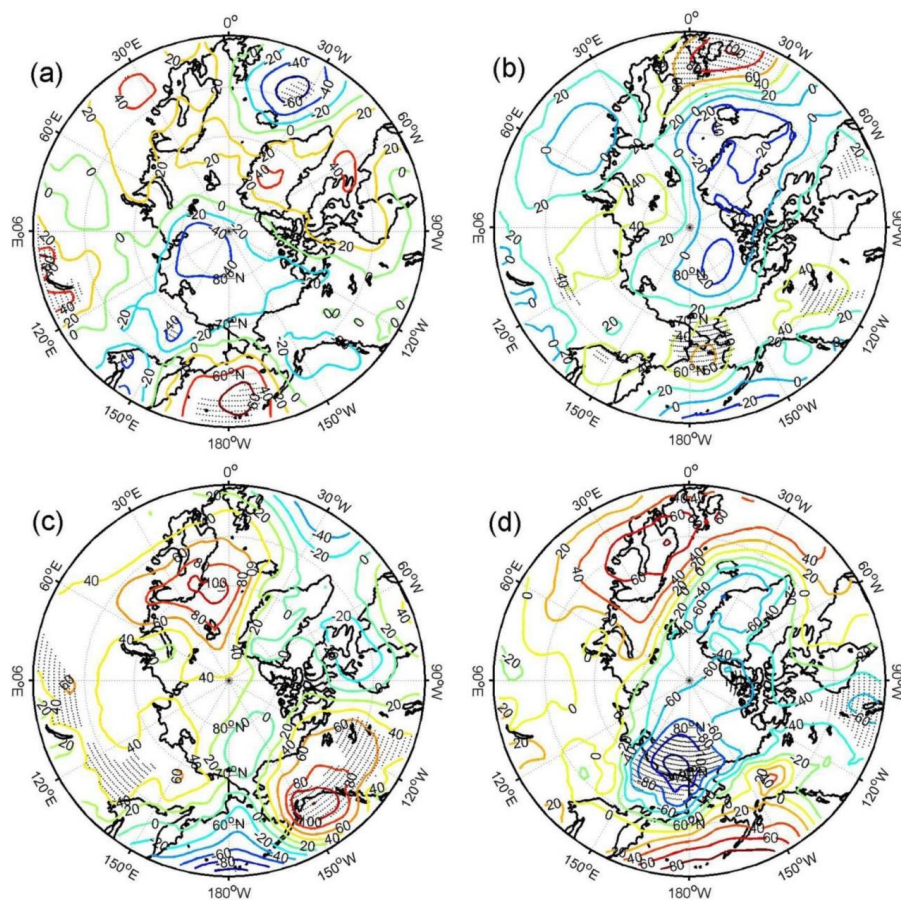


Figure 8. Regression maps of 500-hPa geopotential height (gpm) into the time series of the first (a), (c) and second (b), (d) mode of summer (a), (b) and autumn (c), (d) North Pacific SST anomalies. Dotted regions indicate above 95% confidence level.



659



660

661 Figure 9. The same as Figure 8, but for mean sea level pressure (MSLP) (Pascal).

662

663

664

665

666

667

668

669

670

671

672

673

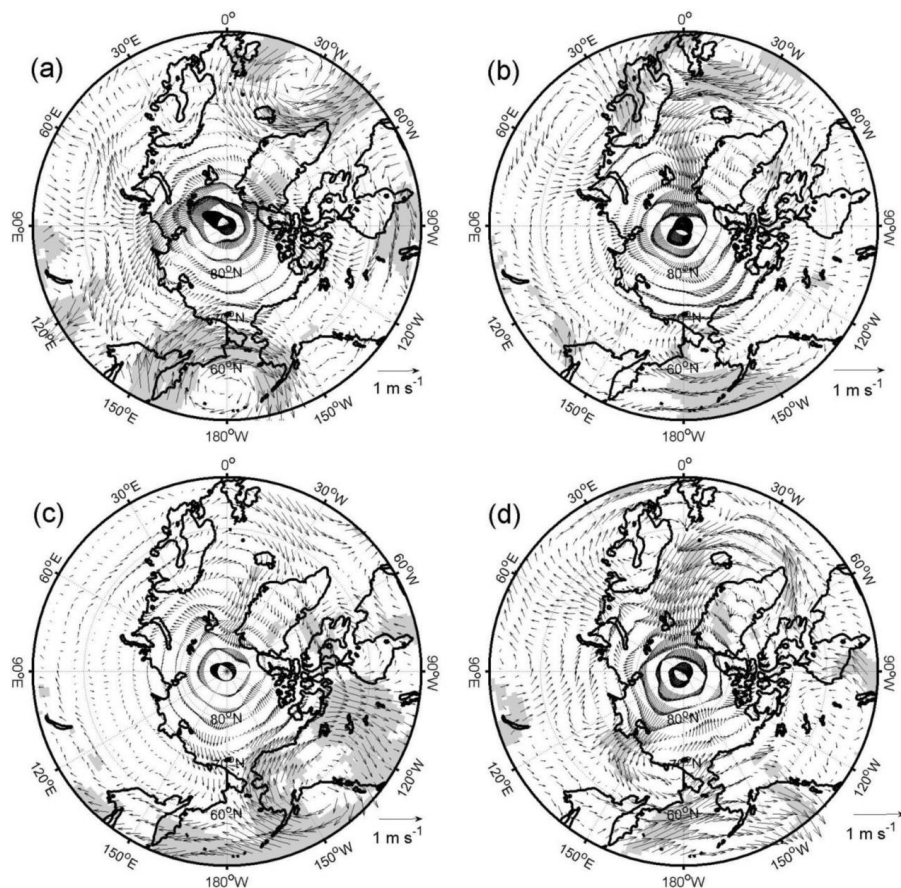
674

675

676



677



678

679 Figure 10. The same as Figure 8, but for 850-hPa wind field.

680

681

682

683

684

685

686

687

688

689

690

691

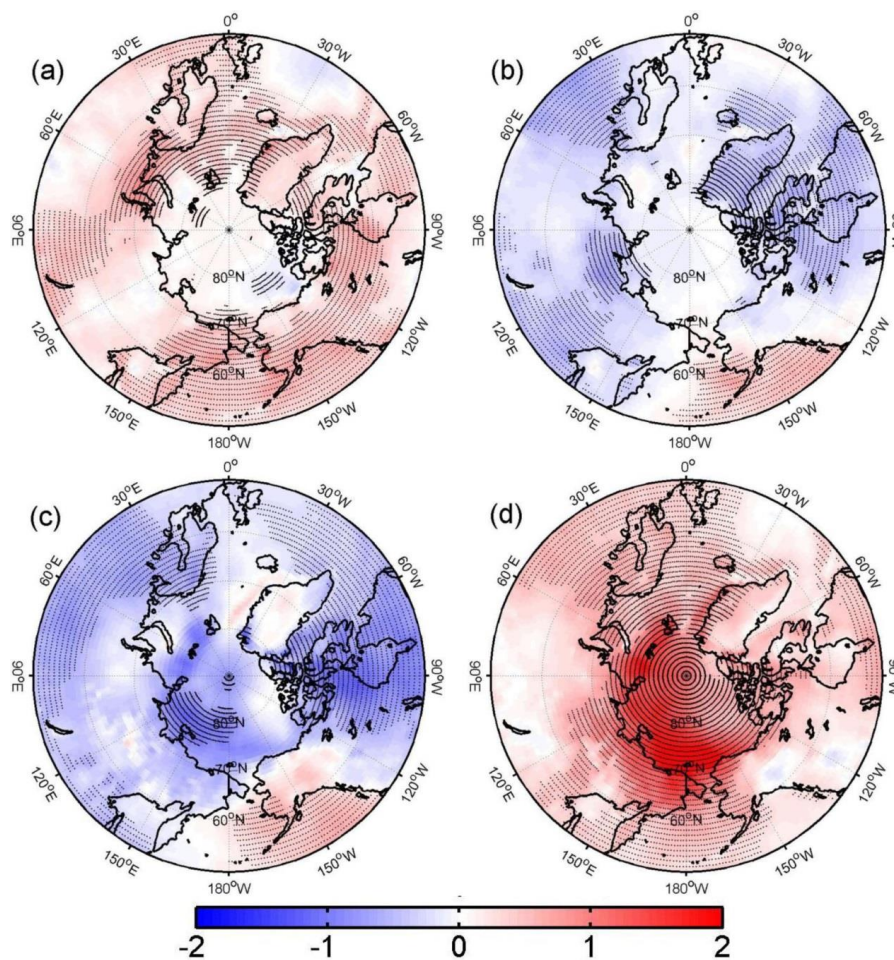
692

693

694



695



696

697 Figure 11. The same as Figure 8, but for surface air temperature ($^{\circ}\text{C}$).

698

699